Biological Journal of the Linnean Society, 2009, **98**, 540–555. With 8 figures

The rowing-to-flapping transition: ontogenetic changes in gill-plate kinematics in the nymphal mayfly *Centroptilum triangulifer* (Ephemeroptera, Baetidae)

ANDREW T. SENSENIG[1]*, KENNETH T. KIGER[2] and JEFFREY W. SHULTZ[1]

[1]*Department of Entomology, University of Maryland, College Park, MD 20742, USA*
[2]*Department of Mechanical Engineering, University of Maryland, College Park, MD 20742, USA*

Submitted 18 March 2009; accepted for publication 11 June 2009

Comparative studies encompassing a wide range of aquatic animals have shown that rowing is exclusively used at low Reynolds numbers ($Re < 1$), whereas flapping is predominantly used at $Re > 100$, although few studies have been undertaken to document the transition in individual species that traverse the intermediate *Re* regime using a single set of appendages. Thus, it is not generally known whether a gradual increase in *Re* within a system results in a gradual or sudden shift between rowing and flapping. In the present study, we document ventilatory kinematics of a nymphal mayfly *Centroptilum triangulifer* that develops using a serial array of seven pairs of abdominal gill plates and operates at Reynolds numbers in the range 2–22 during ontogeny. We found that some kinematic variables (stroke frequency and metachronal phase lag) did not change during ontogeny but that others changed substantially. Specifically, gill kinematics in small instars used strokes with large pitch and stroke-plane deviations, whereas larger instars used strokes with minimal pitch and minimal stroke-plane deviation. Gills in larger instars also acquired an intrinsic hinge that allowed passive asymmetric movement between half strokes. Net flow in small animals was directed ventrally and essentially parallel to the stroke plane (i.e. rowing), whereas net flow in large animals was directed dorsally and essentially transverse to the stroke plane (i.e. flapping). The change in whole-gill kinematics from rowing to flapping occurred across a narrow *Re* range (3–8), which suggests a possible hydrodynamic demarcation between rowing and flapping. *Biological Journal of the Linnean Society*, 2009, **98**, 540–555.

ADDITIONAL KEYWORDS: aquatic insects – growth – intermediate Reynolds number – ventilation.

INTRODUCTION

Animals have evolved diverse mechanisms to generate currents for ventilation, feeding and locomotion, but there are mechanical trends associated with animal size that transcend differences in morphology and phylogeny (Strathmann, 1993; Walker, 2002). The Reynolds number ($Re = UL/\eta$, where U is a reference velocity scale, L is a reference length scale and η is the kinematic viscosity) is a key dimensionless parameter in fluid dynamics that reflects the relative importance of the fluid's inertia and viscosity (i.e. internal friction). Inertial effects dominate flow at large sizes and high velocities ($Re >> 1$), and viscous forces control flow dynamics at small sizes or relatively low speeds ($Re << 1$). The basic mechanisms operating at the biological extremes of *Re* are relatively well understood, as exemplified by studies based on inviscid models for relatively fast and/or large swimming or flying vertebrates ($Re > 1000$) (Daniel, Jordan & Grunbaum, 1992; Motani, 2002; Spedding, Rosen & Hedenstrom, 2003) as well as classical studies of viscous flow around flagella and cilia ($Re << 1$) (Taylor, 1951; Gray & Hancock, 1955; Lighthill, 1976; Brennen & Winet, 1977). Definitions of the less-studied intermediate *Re* regime vary among workers (Webb & Weihs, 1986; Daniel & Webb, 1987; Daniel *et al.*, 1992; Fuiman & Batty, 1997;

*Corresponding author. Current address: Department of Biology, University of Akron, Akron, OH 44325, USA. E-mail: andrew6@akron.edu

Walker, 2002), but all generally encompass *Re* = 1–20. This regime spans a very narrow but important part of the biologically relevant *Re* spectrum. Comparative studies and computer simulations (Walker, 2002; Childress & Dudley, 2004) indicate that organisms at the lower end of the regime should exclusively use rowing strokes, and those at the upper end should tend to use flapping strokes, due to benefits in propulsive efficiency or viscous limitations on thrust production by simple flapping motions. Consequently, studies of species that transit this region, either ontogenetically or behaviourally, may be important for establishing how aquatic animals achieve the rowing-to-flapping transition and whether this transition is sudden or gradual.

It is important for purpose of the present study to define flapping and rowing. Appendages generate force in fluids through net action of the viscous stress and pressure distribution across its surface. At high *Re*, the net viscous contribution is typically small relative to that of pressure, which is effectively generated by the change in inertia of the fluid surrounding the appendage. Under these conditions, circulatory lift force is the dominant effect, so that an appendage translating at a small angle of attack relative to oncoming flow experiences a large force perpendicular to this flow (lift). Because of the unsteady motion, a component of the instantaneous lift is directed along the flow, such that there is a net production of positive thrust. This corresponds to a simplified view of the case for a flapping type motion and, in the present study, we take pure flapping to occur when appendage strokes are perpendicular to flow or to the direction of motion (Fig. 1). By contrast, at very low *Re*, viscous stresses become dominant, and inviscid mechanisms such as circulatory lift become ineffective. Under these conditions, a net thrust is generated by separating strokes into a power half-stroke that produces high thrust through drag, and a recovery half-stroke that reduces drag via changes in appendage shape, orientation or speed (Kohlhage & Yager, 1994; van Duren & Videler, 2003). A rowing type motion then corresponds to an appendage stoke that occurs in the direction of flow or net thrust. It should be noted that rowing strokes and mechanisms are also possible at higher *Re* (the oar of a rowboat being a classic example), but here the inertia reaction of the fluid, and not viscous forces, is responsible for the thrust. Typically, flapping is more prevalent at high *Re* conditions, as speculated for a net gain in efficiency (Walker, 2002; Walker & Westneat, 2002).

The shift from rowing to flapping in a single organism is analogous to some gait changes in legged terrestrial animals that alter their motor pattern with increasing speed to increase the energetic efficiency of travel (Heglund, Taylor & McMahon, 1974; Hoyt & Taylor, 1981; Heglund & Taylor, 1988; Alexander, 1989). Certain transitions in swimming mechanisms have been called 'gait' changes, notably the change from continuous to burst-and-coast swimming (Weihs, 1974; Videler & Weihs, 1982) and pectoral to caudal fin-powered swimming (Drucker, 1996; Cannas *et al.*, 2006) in fish. Such transitions have been identified only in organisms operating at relatively high Reynolds numbers ($Re > 100$). To our knowledge, no shifts between rowing and flapping have yet been identified within a single appendage set during changes in propulsive speed or over ontogeny, even though multiple studies predict that such a shift should occur.

In the present study, we use a novel oscillating appendage system, namely the abdominal gill array of mayfly nymphs, to determine whether a rowing-to-flapping gait change occurs and, if so, whether this change occurs abruptly or gradually with increasing Reynolds number. The nymphal mayfly, *Centroptilum triangulifer* (Ephemeroptera, Baetidae), grows through the intermediate *Re* regime while maintaining an array of seven pairs of plate-like gills (Fig. 2). Kinematic analysis of high-speed (1 kHz) videos revealed an apparent gait shift near frequency Reynolds number, $Re_f = fL_g^2/\eta = 5$, which consisted of a transition of high to low asymmetry in several stroke

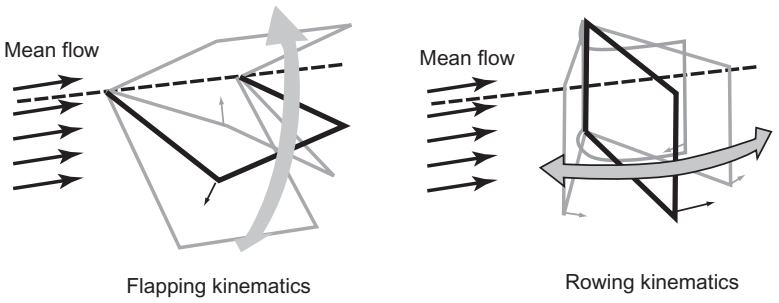

Figure 1. Schematic illustration of kinematic distinction of flapping versus rowing type motions (*sensu* Walker and Westneat, 2002).

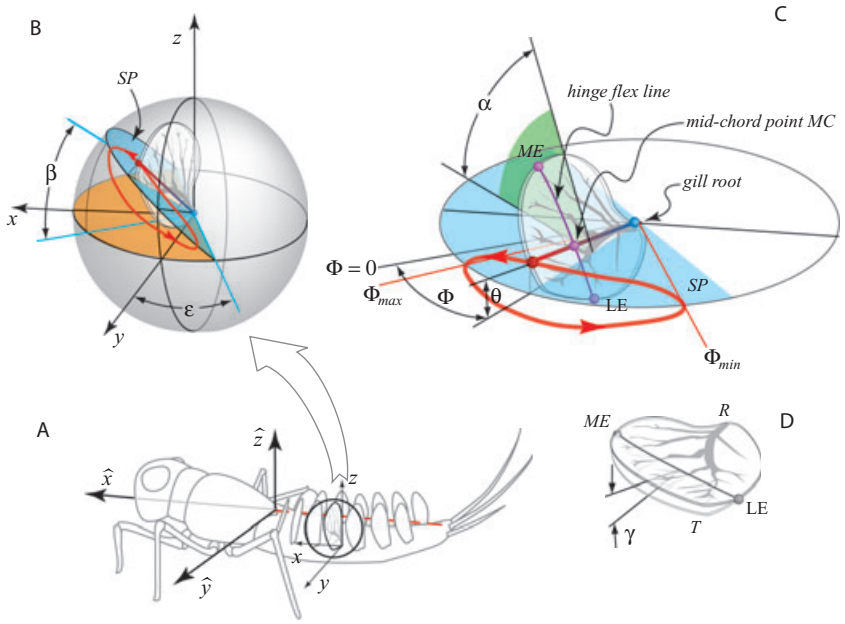

Figure 2. Spatial axes and angles used in characterizing gill-plate kinematics in the nymphal mayfly. A, diagrammatic mayfly nymph from an oblique lateral perspective showing spatial coordinates relative to the body ($\hat{x}$, anterior–posterior axis; $\hat{y}$, transverse axis; $\hat{z}$, dorsal–ventral axis) and parallel coordinates originating at the gill root (x, y, z). B, C, key kinematic parameters. The stroke plane (SP) for each cycle (indicated in blue) is defined by three points: the gill root and the anterior and posterior extrema of the gill mid-hinge point. The orientation of the SP is defined by the stroke-plane inclination angle (β), measured between the SP and the horizontal (x–y) plane within a mutually orthogonal plane, and the stroke-plane lateral offset angle (ε), which indicates where the SP crosses the horizontal (x–y) plane. The instantaneous position of the mid-chord point (path indicated by the red curve) is then given by the combination of the stroke angle, Φ, and stroke-plane deviation, θ, which measures the angular displacement along and normal to the SP, respectively. The stroke angle origin ($\Phi = 0$) is referenced to the position where the SP intersects the transverse-vertical (y–z) plane, and the respective posterior/anterior excursion limits are given by Φ_{min}/Φ_{max}. The orientation of the gill plate is referred to as the pitch, α, which is defined as the angle between the gill plate and the SP, as measured in a mutually orthogonal plane. D, gills in larger nymphs have a distinct transverse hinge flex line. The hinge angle, γ, is defined as the deflection of the distal gill plate (flap) from the nominally planar configuration. The hinge angle is positive when the hinge is flexed posteriorly and negative when flexed anteriorly.

parameters. In this definition of the Reynolds number, the velocity scale is determined by the product of the stroke frequency in Hertz (f) and the length of the gill plate (L_g). Both the magnitude of the range of gill pitch and deviation from the mean stroke plane decreased abruptly with increasing Re_f. These changes in gill-plate kinematics were accompanied by the development of a passively oscillating distal flap and a significant shift in net flow from a direction approximately parallel to the stroke plane to one more perpendicular to the stroke plane. These ontogenetic transitions suggest a possible hydrodynamic limit at low Re_f in early instars that is reflected by a relatively rapid switch between two gaits corresponding to the basic categories of rowing and flapping. This result is consistent with simulation- and model-based results predicting a rapid rather than gradual change in appendage kinematics with gradually increasing Re_f. The results obtained in the present study suggest that the apparent absence of aquatic organisms that use stroke kinematics intermediate between rowing and flapping results from selection against hydrodynamic or energetic inefficiency rather than inadequate comparative sampling from species occupying the intermediate *Re* regime.

MATERIAL AND METHODS

STUDY ORGANISM AND CINEMATOGRAPHY

Centroptilum triangulifer is a common parthenogenetic mayfly of slow-flowing streams in eastern North America (Sweeney, Funk & Standley, 1992; Funk, Jackson & Sweeney, 2006). Eggs of *C. triangulifer*

were obtained from a stock population of Stroud Water Research Center (Avondale, PA, USA), and nymphs were reared at 20 °C in 1 cm of water within covered Petri dishes. After several instars (15 days), nymphs were approximately 1 mm long and single lamellar gills developed on the lateral edges of seven adjacent abdominal segments. Gill pairs of each segment (1–7) were designated by order from anterior to posterior position. At approximately 20 days, nymphs were approximately 2 mm long with actively oscillating gills. On days 20, 21, 23, 25, 27, 28, 35, and 42, a nymph was taken from cultures and used for three-dimensional (3D) kinematic analysis, with two nymphs selected on day 25 (Table 1). The examined size range was 2.0–5.6 mm in length. Body lengths excluded the caudal filaments. Size increased with age, although an individual on day 25 was slightly larger than the nymphs sampled on days 27 and 28. Individuals emerged from the water at approximately 6 mm in length. Individuals were also captured in the Paintbranch Creek, University of Maryland (College Park, MD, USA) in August to October 2006. Only laboratory-reared nymphs ($N = 9$) were used in the 3D kinematic analysis. Wild and laboratory cultured nymphs were not qualitatively different in gill kinematics across corresponding animal sizes, and hence both laboratory-reared ($N = 5$) and wild caught nymphs ($N = 8$) were used in the flow field imaging trials to characterize changes in flow patterns as a function of Re_f.

Experimental set up

Nymphs were removed from water and dried for approximately 1 min on tissue paper. The tip of a minutien pin was dipped into cyanoacrylate and attached dorsally to the nymph's thorax. The other end of the pin was embedded in a mound of petroleum jelly that had been affixed to one wall of a chamber ($20 \times 20 \times 20$ mm) constructed from glass microscope-slide covers. Nymph orientation inside the chamber was manipulated using forceps to position the pin relative to the jelly, so as to suspend the nymph at a typical resting distance from the bottom and at least 7 mm from the dorsal and lateral walls. The chamber's free surface was then covered with a microscope slide to form a complete seal. Water temperature in the chamber was 20 ± 2 °C, and nymphs initiated periods of ventilation as the oxygen diminished. In small nymphs, this occurred in approximately 1 h, whereas large nymphs often began ventilation immediately.

Lateral and dorsal images (4×4 mm field of view) of the ventilating array were captured by two synchronized cameras (Phantom v9; 1632×1200 pixels; V.4, 512×512 pixels) operated at 1000 fps and

Table 1. Size and kinematic data of all nymphs examined

Animal age (days)	L_a (mm)	L_g (mm)	L_{rs} (mm)	f (Hz)	Re_f	α mean gill 4 (°)	α range gill 4 (°)	α range gill 4 (°) SD	$\Phi_{max} - \Phi_{min}$ (°)	$\Phi_{max} - \Phi_{min}$ SD	β (°)	ε (°)	γ range (°)	γ range (°) SD	θ range (°) gill 4	phase lag gill 4–5
20	2	0.25	0.16	34	2.1	70	37	3.4	30	0.9	55	81	16.54	2.41	13.11	0.26
21	2.30	0.30	0.17	26	2.3	71	36	1.9	49	1.2	52	80	18.16	2.93	11.55	0.19
23	2.90	0.50	0.24	20	5.0	60	23	3.5	40	0.2	65	79	23.87	0.40	7.61	0.28
25	3.15	0.65	0.24	20	8.4	93	10	0.9	36	0.7	68	87	40.62	1.75	3.05	0.16
25	3.50	0.51	0.24	25	6.5	87	9	0.5	40	0.4	57	74	64.26	3.55	5.01	0.17
27	3.29	0.58	0.23	25	8.4	100	4	1.6	31	1.2	77	79	43.04	4.89	4.16	0.17
28	3.33	0.65	0.23	29	12.2	104	11	1.8	28	2.4	60	80	57.64	9.48	4.13	0.18
35	5.18	0.82	0.39	30	20.1	87	10	0.7	22	0.6	74	81	50.39	5.10	2.50	0.20
42	5.64	0.77	0.41	37	21.6	86	8	2.1	24	0.6	61	86	61	7.03	1.82	0.23

L_g, gill 4 length; L_a, animal length not including caudal filaments; L_{rs}, root separation distance; f, frequency; Re_f, frequency Reynolds number; Φmax – Φmin, stroke range; SD, standard deviation of fourstrokes; β, stroke-plane inclination angle; ε, stroke-plane lateral offset angle; γ, hinge angle; θ, stroke-plane deviation angle.

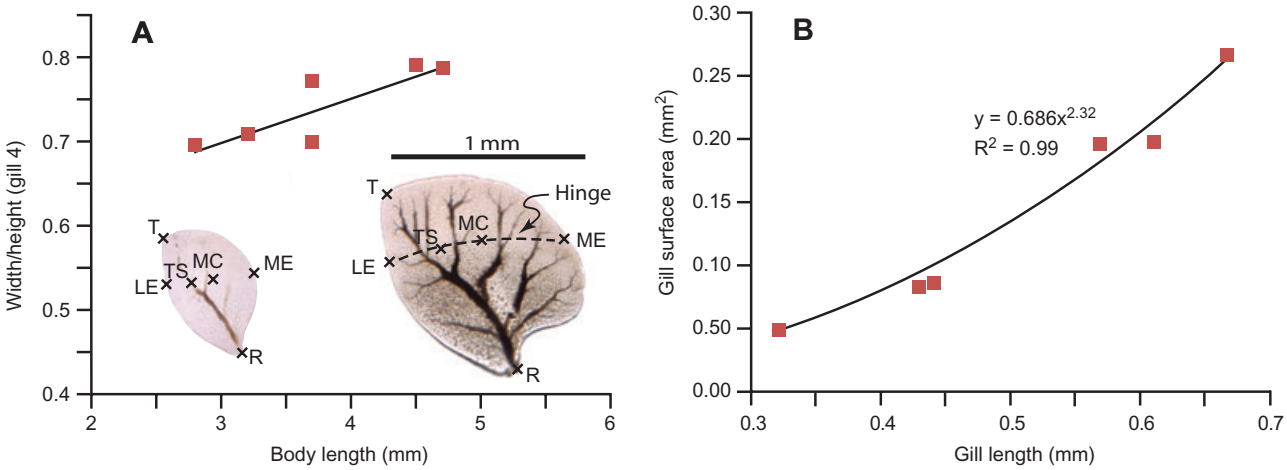

Figure 3. A, ratio of gill 4 (width/height). B, gill 4 surface area as a function of gill length.

attached to Leica dissecting microscopes (×30 magnification zoom lens). The cameras were adjusted to orthogonal positions (within 5°). Nymphs were front illuminated for each camera view with two Leica gooseneck lamps (each lamp box with two fiber optic necks, and a 100 W incandescent bulb). A separate glass chamber containing a 1-mm grid provided a two-dimensional (2D) calibration image for the dorsal perspective. This 2D calibration scale was used to define the length and width of the abdomen, with the length providing the scale factor for the lateral perspective. The resulting movie files were imported to a 3D motion analysis program (Motus Peak Performance, version 7). A 3D spatial calibration was performed using the animal's body (with known length and width) as a calibration object in combination with the 2D calibration described above. This nymph-based calibration object was defined as a virtual box with vertices formed by the roots of gills 2 and 6 on both sides of the abdomen and the height of the resting gills. The gills on the far side of the body, although out of focus in the lateral image, provided a measure of roll and yaw for the calibration box, and did not indicate any significant parallax in the camera lens system. The object space defined by this calibration was self-consistent to the extent that points could be located to within 0.001 mm in each dimension. Along with the root location (R), the tip (T), medial edge point (ME), and lateral edge point (LE) of each gill was digitized in each frame (see landmarks defined in Figs 2, 3). Uncertainty in the values of the kinematic parameters was derived from both the spatial calibration and landmark ambiguity of the multiple points that define each parameter. Spatial calibration and landmark ambiguity errors were quantified separately. The spatial calibration contribution was quantified by comparing the pitch angles of the same sequence of strokes before and after intentional skewing of the virtual calibration box, where the skewing was the maximum possible as a result of ambiguity in location of the box vertices. This resulted in a shift of pitch angle of 2.2 ± 3.9° (mean ± SD, $N = 5$ pitch extrema) in the smallest nymph and 0.7 ± 0.2° in the largest nymph. The landmark ambiguity contribution to the error was quantified by comparing the pitch angle extrema of the same sequence of strokes ($N = 5$ periods) under two independent digitizations of the gill landmarks. Because of the large pitching motion of the small nymph gill plates, landmark digitization error accounted for approximately 18% (–0.4 ± 6.5° versus 37°) of the full pitch range. Landmark digitization error produced a mean offset of the pitch in the largest nymph similar to the full pitch range at that size (6 ± 1.2° versus 8°), but the pitch range itself did not change. Hinge angle in the largest nymph shifted 3 ± 2.8° ($N = 5$ periods) as a result of landmark ambiguity, but less than 1° as a result of spatial calibration error.

After the high speed images of the animals were captured, hollow glass beads (mean diameter of 11 μm; Potters Industries, Grade 110P8) were added to the water for flow-field analysis. Flow in the vertical plane just lateral to the abdomen was quantified using planar cinematographic particle image velocimetry (PIV) (1000 fps, exposure time 950 μs). We used a 400 mm (focal length) plan-convex lens and 63 mm (focal length) plan-cylindrical lens to generate a light sheet from the beam of a continuous Argon ion laser (maximum power 2 W; Coherent Innova 90). In the filming area, the light sheet was 20 mm wide and 0.2 mm thick. The size of the initial sub-image for the PIV ensemble correlation procedure was 128 × 128 pixels, and was reduced to 32 × 32 for the second and

final correlation. Overlap between sub-images was 50%. The influence of light scattered by the gill plate was removed by subtracting the mean image for the local ensemble prior to computation of the correlation. Altogether, the inter-gill flow field of 13 ventilating individuals was resolved through the PIV ensemble-correlation, including eight animals not observed in the 3D study.

Gill-plate kinematics

The 2D raw coordinates from digitizing each perspective were Butterworth filtered (100 Hz cutoff) and transformed to 3D coordinates (Motus Peak Performance, version 7). The 3D-transformed coordinates were analysed in MATLAB, R2006b. The mobile gills of animals greater than 3 mm body length bend at a hinge line that demarcates proximal and distal regions of the gill. This hinge line lies approximately parallel to the horizontal *x–y* plane (Fig. 2). The medial–dorsal end and lateral–ventral end of the hinge line were clearly defined points in the bending gills, which, along with the gill root, provided three convenient points in which to reliably define a proximal plate for the gill [referred to earlier as the ME, LE and R, respectively]. We digitized the analogous points in the animals with nonhinged gills (body length < 3 mm). The stroke plane (Φ) of wings in flying insects is usually defined as the plane that contains the wing root and the most anterior and posterior positions reached by the wing tip (Dudley 2000). Because of the tip flexion in the largest animals, we used the trajectory of the midchord point (MC, taken to be the bisector of the medial edge, ME, and lateral edge, LE, points) to define the stroke plane in all the animals (Fig. 2). Using a stroke plane defined by the trajectory of an alternative point (TS, subdistal trachea point), calculated as the intersection of the ME/LE line and T/R line (Fig. 3), produced slightly different kinematic results. For the smallest nymph, using the point TS rather than the midchord decreased the pitch range from 37° to 33°, and, for the largest nymph, increased the pitch range from 8° to 12°. The stroke plane can be described by an inclination angle (β) and lateral offset angle (ε), where β is the angle between the stroke plane and the *x–y* (coronal) plane, and ε is the angle between the stroke plane intersection with the *x–y* (coronal) plane and the *y–z* (transverse) plane (Fig. 2). The *x–y* (coronal) plane of the animal was specified as that containing the roots of gills 2 and 6 on both sides, whereas the *y–z* (transverse) plane was specified by the roots of gill 4 of both sides, and the dorsal and ventral abdominal surfaces associated with gill 4. Pitch (α) was defined as the angle between the stroke plane (Φ) and the plane formed by the proximal plate of the gill, measured in the plane orthogonal to both surfaces. Stroke plane deviation angle (θ) was the angle between the root-midchord line and the stroke plane (Φ), and was considered to be positive if medial to the stroke plane, and negative if lateral. The hinge angle (γ) was the angle between the proximal and distal gill plates. This quantity was reported even for the three smallest animals that had no visible hinge line, and minimal, if any, bending. In the case of the three smallest animals, any variation of the hinge angle from 0° primarily represented the accumulated error produced by the digitization of the three points that defined the distal plate. Phase lag was calculated by auto-correlating the time-varying kinematic parameters (i.e. pitch and stroke angle for the three smallest nymphs or hinge and stroke angle for the five largest nymphs) between adjacent gills over four stroke cycles. We report the average of these two measures of phase lag.

Re_f was derived from the gill length in mm (L), oscillation frequency in Hz (f) and kinematic viscosity in cSt (η): $Re_f = L^2 f \eta^{-1}$ (Borrell, Goldbogen & Dudley, 2005).We performed linear regression analyses to determine the effect of size on all the kinematic parameters using both Re_f and body length as the independent variable (Microsoft Excel). We determined that using animal length instead of Re_f as the independent variable in the regression did not change the statistical significance of any of the tests; therefore, we report the statistical results for only one of these independent variables.

To assess the potential for drag asymmetry between half strokes for individual gills, we calculated a volumetric sweep rate:

$$\mathrm{VSR} = [A_{\mathrm{prox}} n_{\mathrm{prox}} + A_{\mathrm{flap}} n_{\mathrm{flap}}] \cdot v$$

where n is the unit normal vector of the gill plate surface (the gill has been divided into a proximal plate and a distal flap surface), A is the surface area of the given portion of the gill plate, and v is the velocity of gill plate at the mid-span position. It should be stressed that this is a purely kinematic quantity that was constructed to display the combined effects of orientation and velocity because it is difficult to make a direct kinematic connection to the drag within the range of Reynolds numbers under consideration. This is a result of the different scaling required by the viscous and inertial limits: in the creeping flow limit, drag is directly proportional to the viscosity, length, velocity and orientation, $F_D(Re \to 0) = F_D(\mu,\ l,\ v,\ \alpha)$; whereas, in the inertial limit, it depends on the density, area, square of the velocity and orientation; $F_D(Re \to \infty) = F_D(\rho,\ l^2,\ v^2,\ \alpha)$. For these reasons, the drag coefficients and velocity exponents required to quantify the relationship between kinematics and drag must be determined

individually for each case, so that drag cannot be immediately determined by speed and frontal area alone. Nevertheless, VSR highlights the potential for drag asymmetry between half strokes, as a result of its combination of length, velocity, and orientation. The ratio of the integrated VSR between the power-stroke and return stroke is an additional measure of half-stroke asymmetry.

To confirm that the stroke patterns were not artefacts of mechanical restraint, lateral wall effects, or the genetic strains of the animals, 22 nymphs (1.7–6.1 mm body length) were captured in the Paintbranch Creek, University of Maryland (College Park, MD, USA) in August to October 2006, and high-speed images were taken within 24 h, whereas the unrestrained nymphs ventilated in a 1-cm-deep Petri dish. The gill kinematics of all nymphs less than 2.5 mm head-to-tail length ($N = 4$ out of 22 nymphs, 31–45 Hz, *Re* range ~ 2–3.8) could be easily classed as having high-pitch movements and low-hinge amplitude compared to the larger animals from the sample, which was qualitatively similar to that noted in the detailed kinematic analysis.

Gill-plate morphology

Nymphs from laboratory Petri-dish cultures were killed in EtOH and dissected. Gill 4 from each animal was placed between a microscope slide and coverslip and photographed (Diagnostic Instruments Spot32 camera on a Leica compound scope; ×100 total magnification) before the alcohol evaporated. A length scale was captured by separately photographing a Leica stage micrometer with 1-μm markings. Length, width, and surface area were measured for each gill (Adobe Photoshop, version 10.0). The aspect ratio, $AR = L_g^2/SA$, where gill length L_g and surface area SA, was determined for each gill.

RESULTS

Generalized kinematics of the gill array

Suspended nymphs attempted to grip the glass substrate and occasionally tried to walk. Attempted swimming was observed and consisted of dorsal–ventral undulation of the abdomen with the gills retracted and held tightly against the abdomen. At rest, gills were always held in the fully protracted (most anterior) position. During ventilation, the body was typically held in a dorsal concave position, with the head and most posterior abdominal segments raised about a half-abdomen-width higher than the middle abdominal segments (Fig. 2). At rest, the seven gill pairs extended from the abdomen, so that the root-midchord segment was oriented at a stroke angle of approximately 0° (Fig. 2). The gill pair of each segment always moved symmetrically and in synchrony. Gill 7 (the most posterior gill pair) never actively moved during ventilation. Ventilation was always initiated with retraction of gill 6. Gill 5 began retraction once gill 6 reached its most posterior position. The metachronal wave of activation traveled anteriorly to gill 1. The first retraction of gill 2 occurred in near synchrony with the second retraction of gill 6. The range of each stroke increased gradually, and required six and 11 full strokes in the two largest nymphs to achieve steady state, but only three cycles in the smaller nymphs. Ventilation continued for several dozen strokes up to indefinitely long periods of time. Gill 7 oscillated through only a small range of movements ($\Phi_{max} - \Phi_{min} < 5°$ and pitch < 10°) that was likely a passive response to the fluid motion produced by gill 6.

Oscillation frequencies were in the range 20–36 Hz (Table 1), with no significant trend associated with Re_f ($r^2 = 0.23$, $F_{1,7} = 2.11$, $P = 0.19$). The phase lag between adjacent gills also did not change significantly with Re_f, varying in the range 0.17–0.26° (61–94°) ($r^2 = 0.01$, $F_{1,7} = 0.08$, $P = 0.78$). Stroke plane inclination of gill 4 was $\beta = 63 \pm 8°$ (range 52–77°) across animals and did not change with Re_f ($r^2 = 0.17$, $F_{1,7} = 1.49$, $P = 0.27$). The lateral offset angle of the stroke plane from the sagittal plane was $\varepsilon = 81 \pm 4°$ (range 74° to 86°, $r^2 = 0.20$, $F_{1,7} = 1.8$, $P = 0.22$). Both the transient and steady-state stroke kinematics were usually repeatable, although occasional digressions occurred in isolated gills in some individuals. These unusual strokes consisted of slightly higher or lower stroke ranges (changes in the order of 10°) and/or slightly delayed phasic activation. We performed statistical analysis only on stroke sequences that were repeatable to the extent that inter-stroke variation was less than the digitization error. The kinematics of only steady-state sequences are reported here. The nymphs used at least two different ventilation strategies as a function of Re_f, with the largest and smallest nymphs exhibiting the extreme development of each strategy, and hence these are described in detail here. One nymph of intermediate size ($Re_f = 5$) was identified as potentially mixing strategies in our 3D study (intermediate level of pitch variation but no hinge development), and several other unrestrained animals of intermediate size used such intermediate kinematics while ventilating in the Petri dish.

Kinematics specific to nymphs with $Re_F < 5$

Gills 2–6 underwent large changes in pitch during the stroke by rotating about the root-tip line (Figs 4A, 5A–F). During gill retraction (posterior–ventral movement), the flat posterior surface of the plate was presented more or less orthogonal to the direction of

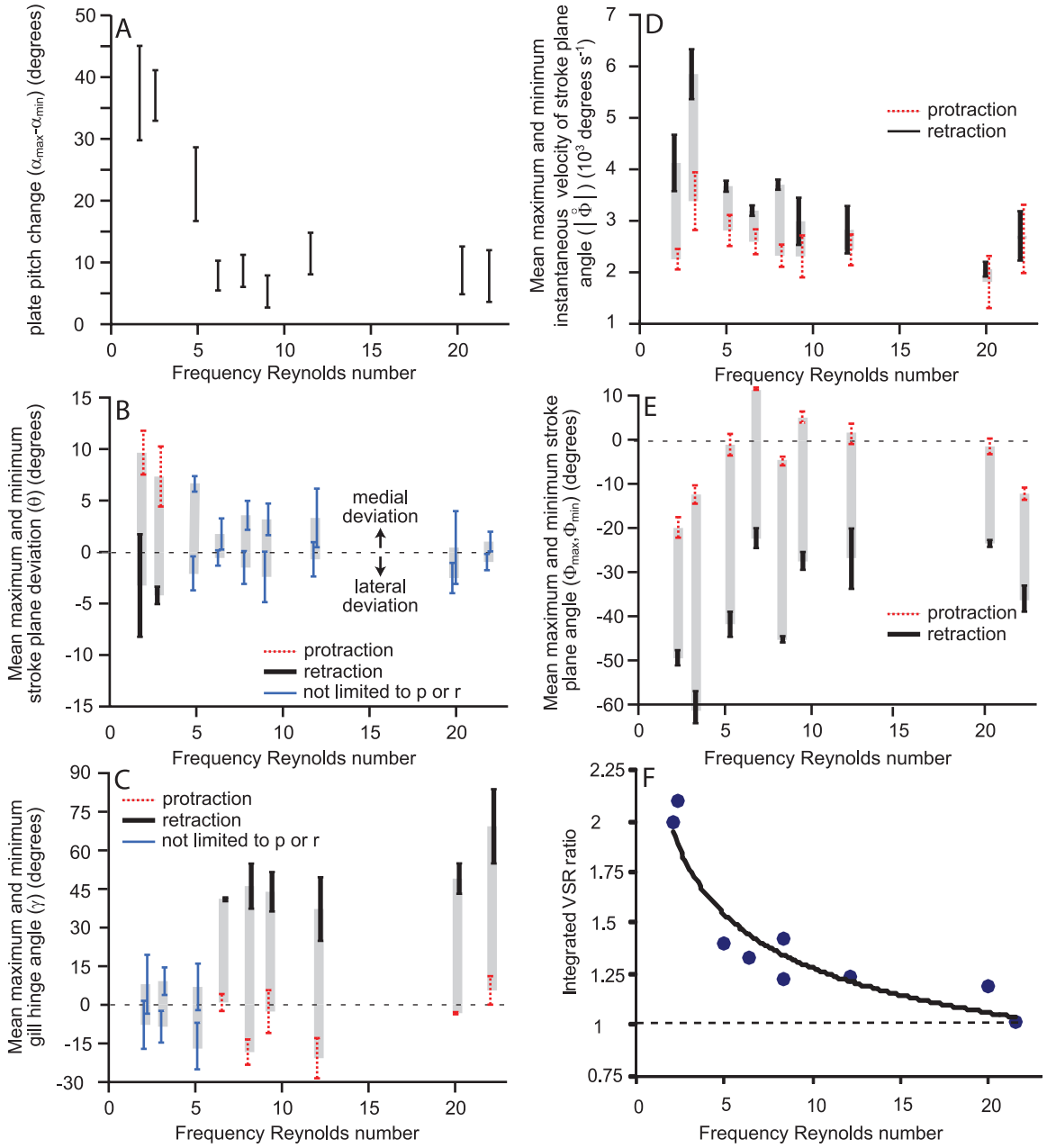

Figure 4. A–F, mean kinematic parameters for gill 4 plotted as a function of frequency Reynolds number (Re_f) for nine individuals. Means were determined from four strokes; error bars indicate ± 2 SD. Extrema indicated by dashed error bars occurred entirely during protraction; extrema indicated by thick error bars occurred entirely during retraction; extrema indicated by thin error bars occurred at various points in the stroke and were not limited to either protraction or retraction.

gill travel, reaching a peak angle of approximately $\alpha = 90°$ and then gradually decreasing pitch in preparation for protraction. During protraction, the gill continued to decrease pitch until mid-stroke, at which time it reached the minimum pitch of approximately 55°. The gill executed protraction (anterior–dorsal travel) at the same time as moving with a more positive stroke-plane deviation angle (θ) (Figs 5B, 6A). Any bending along the long axis of the gill was minimal (< 17°), approximately the digitization accuracy at this small size for this parameter (Fig. 5D). Gill 1 was a shaft-like structure that participated in the metachronal rhythm but with small amplitude of motion. Both VSR and integrated VSR ratio were

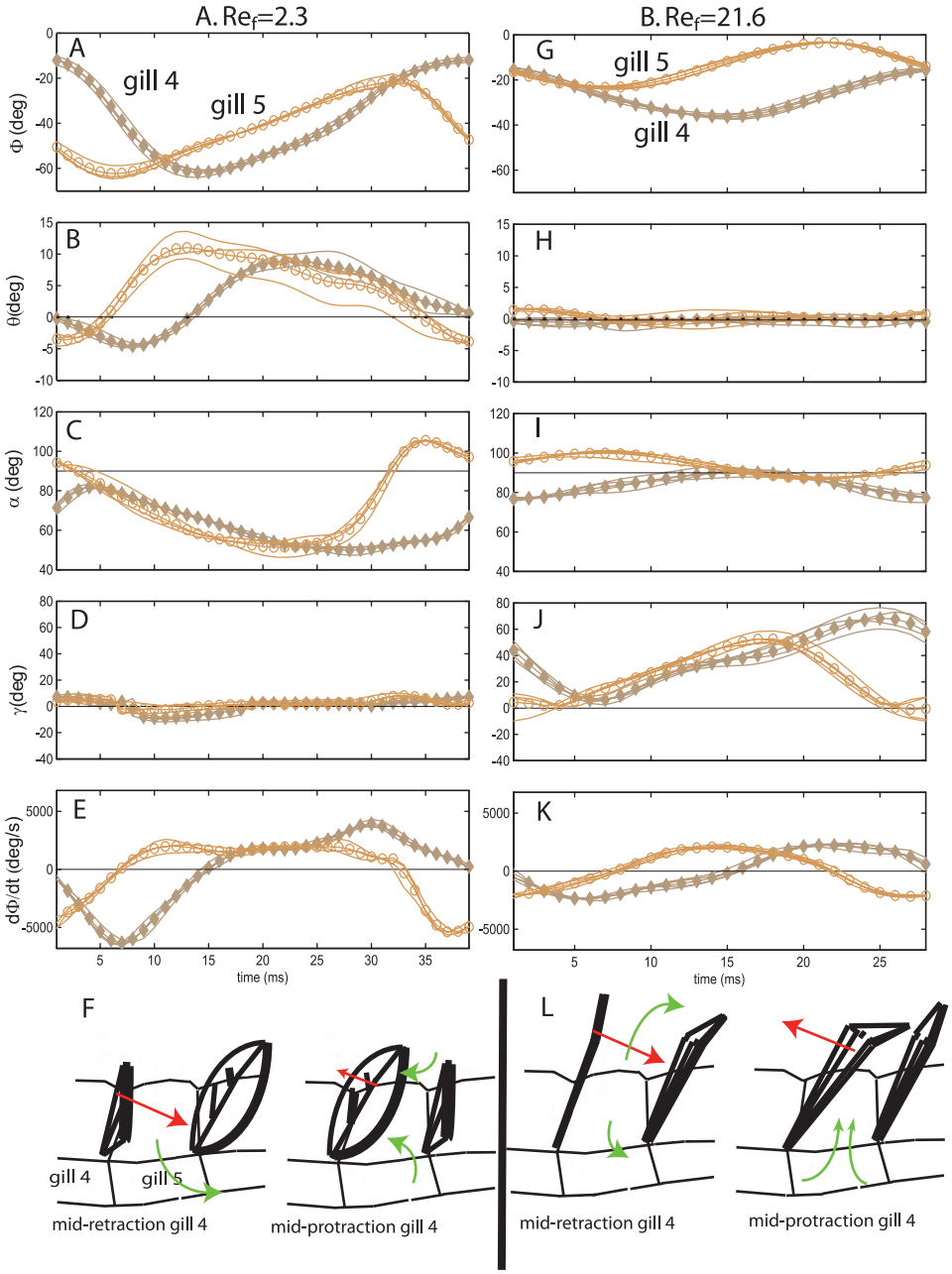

Figure 5. Kinematic parameters for gill 4 (solid diamonds) and gill 5 (open circles) over a stroke cycle. Initiation of retraction of gill 4 marks time = 0 ms. Stroke angle angular velocity is negative during retraction. Re_c number is that associated with the space between the gill indicated and its posterior partner. Thin lines represent individual strokes, whereas thick or dotted line represent mean of individual strokes ($N = 4$). Curved arrows represent the mean flow at that phase, whereas straight arrows indicate gill velocity at that phase. A, B, C, D, E, F, $Re = 2.3$. G, H, I, J, K L, $Re = 21.6$.

highly asymmetric between half-strokes (Figs 4F, 6A), which is a reflection of the strong asymmetries in pitch and stroke velocity between half-cycles. Water flowed from the dorsal to ventral side of the gill array (Fig. 7B), with visual observation also indicating a significant lateral flow component as the fluid exited the array.

KINEMATICS SPECIFIC TO NYMPHS WITH $Re_F > 20$

Nymphs had broad gill plates that retracted and protracted with a relatively constant high-pitch position ($\alpha \sim 90°$; Fig. 5J) and at the same peak speed between halfstrokes (Fig. 5M). The gills had a distinct transverse hinge (Fig. 2D) that created a distal flap, which pointed toward the posterior of the animal

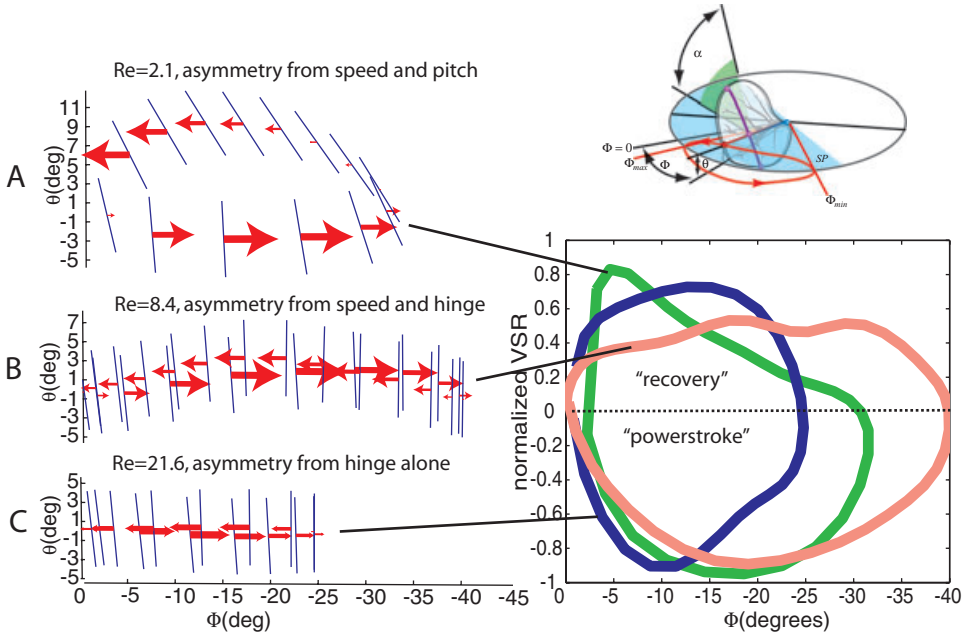

Figure 6. Volumetric sweep rate, defined as VSR = $[A_{prox}\ n_{prox} + A_{flap} n_{flap}]\cdot v$, where A and n are the plan area and unit normal vectors of the gill plate sections (proximal and distal flap) and v is the mid-span velocity of the gill. The inset figures on the left show the orbital trajectories of the gill relative to the stroke plane for three different frequency Reynolds number cases (A, Re = 2.1; B, Re = 8.4; C, Re = 21.6). The orientation of the gill is indicated by the thin line, while the size of the red arrow gives the magnitude of the VSR at the indicated position. The graph on the right depicts a VSR as a function of stroke angle for each of the three cases given. Each case is normalized by its respective maximum VSR magnitude to facilitate relative comparison in stroke symmetry.

when the gills were not oscillating. Resting hinge angle (γ) in the four oldest animals increased from 8° to 29°, but was not significantly correlated with animal length ($r^2 = 0.51$, $F_{1,2} = 2.1$, $P = 0.28$). During ventilation, the flap appeared to move passively under the combined influence of active proximal gill plate movement and hydrodynamic forces. The flap was generally parallel to the proximal plate during retraction, thereby presenting a large projected surface area in the direction of travel, and the flap was bent during protraction so that less area was presented to the travel direction. The stroke range ($\Phi_{max} - \Phi_{min}$) of gill 1 was similar to that of gills 2–6. VSR in these nymphs was only 10% higher during retraction than protraction, and the slight difference was primarily a result of the hinged motion of the distal flap (Fig. 6C). Net flow was directed from the substrate and up through the gill interspaces, and then continued upward with a posterior component, so that an exit jet pointed backward and upward at approximately 45° to the substrate (Fig. 7A).

Gradual and abrupt changes between $Re_F > 20$ (large) and $Re_F < 5$ (small) nymphs

Significant changes over ontogeny occurred in pitch (α), hinge angle (γ), stroke-plane deviation (θ), and retraction angular velocity. The intermediate animal size range of 2.3–3.1 mm ($2.3 < Re_f < 8.4$) marked abrupt changes in several of these parameters. The range of pitch motion over a stroke ($\Delta\alpha = \alpha_{max} - \alpha_{min}$) decreased from 37° to 8°, with instars rapidly decreasing pitch motion over the earliest gilled instars (full dataset linear regression marginal significance, $r^2 = 0.43$, $F_{1,7} = 5.3$, $P = 0.06$, linear regression for distribution of smallest six instars only, $r^2 = 0.94$, $F_{1,4} = 62$, $P = 0.001$) (Fig. 4A). Small nymphs ($Re_f < 5$) utilized a high pitch (90°) during retraction and a significantly reduced pitch (55°) during protraction, whereas the large nymphs did not deviate far from $\alpha = 90°$ (Fig. 5J). Bending at the gill hinge (γ) increased from 17 ± 2° to 61 ± 7° ($r^2 = 0.54$, $F_{1,7} = 8.3$, $P = 0.02$) (Fig. 4C), with an abrupt increase in bending at $Re_f > 6$. Bending was not symmetric about the hinge but was more acute with increasing Re_f ($r^2 = 0.65$, $F_{1,7} = 11$, $P = 0.02$), with the maximum flexion angle ranging from 10° at $Re_f = 2.1$ to 68° at $Re_f = 21.6$. Stroke-plane deviation (θ) decreased with Re_f from 10 ± 3° to 0 ± 2° (Fig. 4B).

Several parameters (ratio of peak protraction to peak retraction speed and the range of stroke motion) changed gradually with Re_f over the entire range of study. Peak angular speed of retraction decreased

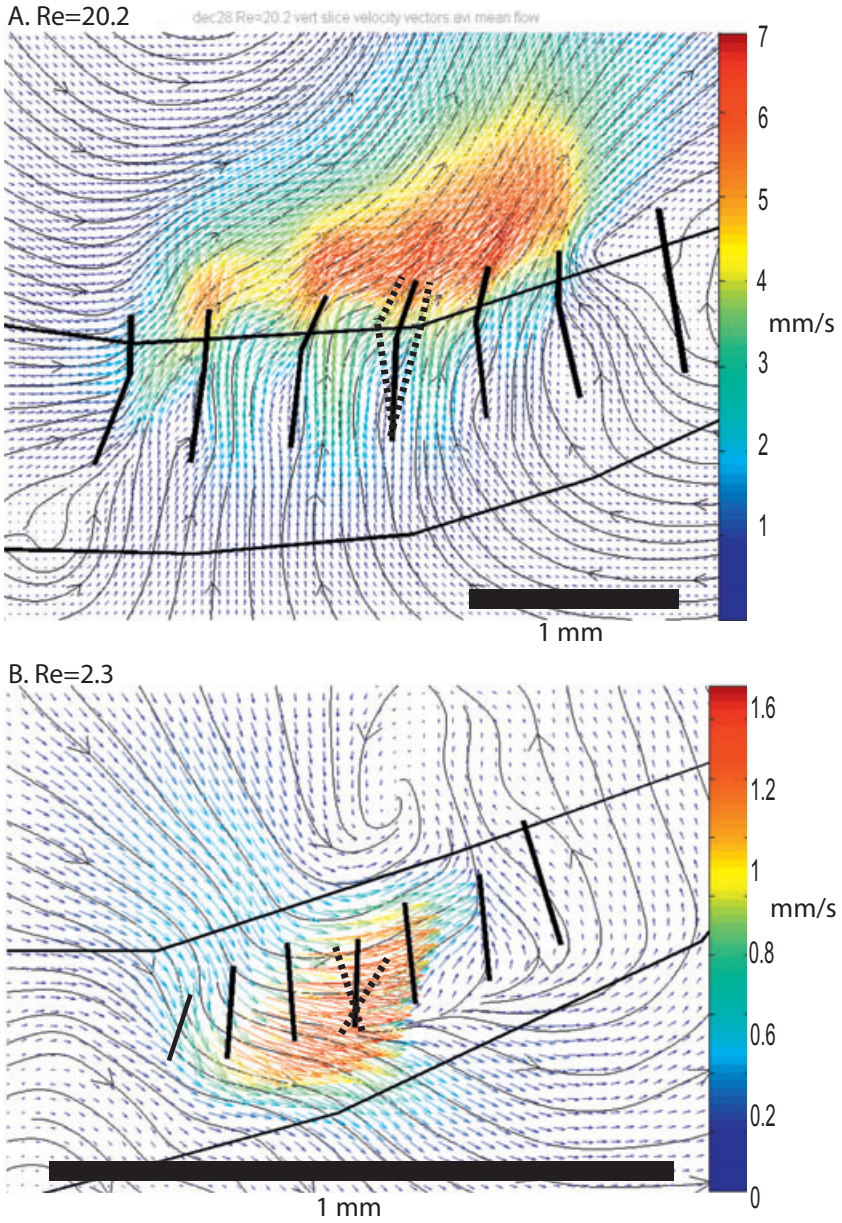

Figure 7. A, flow field through and around the gill array in the vertical plane quantified by ensemble correlation particle image velocimetry (PIV) for frequency Reynolds number (Re_f) = 20.2. Mean gill positions over a stroke cycle for gills 1–7 and abdomen outline shown by solid black lines. Gill 4 protraction and retraction maximal positions shown for both the proximal and distal plates as dotted lines. B, flow field through and around the gill array in the vertical plane quantified by ensemble correlation PIV for Re_f = 2.3. Mean gill positions over a stroke cycle for gills 1–7 and abdomen outline shown by solid black lines. Gill 4 extreme protraction and retraction positions shown as dotted lines. There is no measurable flexion about a hinge in any of the gill plates at this Re_f.

with increasing body length, whereas the protraction speed was relatively constant, a pattern that resulted in equal peak protraction and retraction speeds in the largest animals (Fig. 4D). The ratio of peak protraction to peak retraction speed increased gradually with Re_f ($r^2 = 0.75$, $F_{1,7} = 21$, $P = 0.003$). Stroke range ($\Phi_{max} - \Phi_{min}$) decreased gradually with Re_f ($r^2 = 0.61$, $F_{1,7} = 11$, $P = 0.013$) (Fig. 4E).

For nymphs operating at $Re_f < 5$, VSR was approximately 100% greater during the retraction 'power-stroke' than during recovery (Fig. 6A), and this was entirely a result of the high speed and pitch during

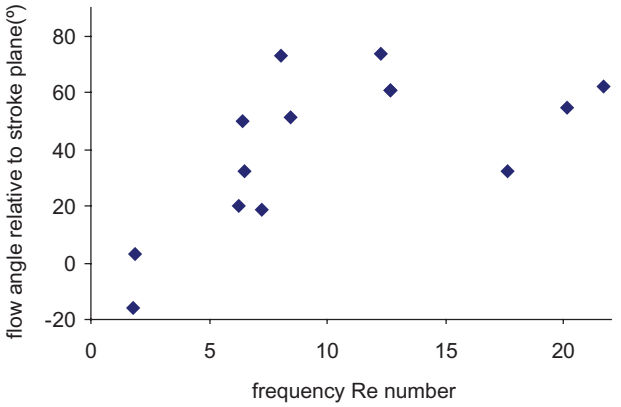

Figure 8. Change in flow direction as a function of frequency Reynolds number (Re_f) for 13 individuals Mean flow direction was calculated as the average of the flow over the entire imaged area. A 90° angle is expected for an idealized flapping stroke, and a 0 degree angle for an idealized rowing stroke. Flow angle increases with Re_f ($r^2 = 0.76$, $F_{1,7} = 22$, $P = 0.002$, linear regress on $Re_f < 12.3$), ($r^2 = 0.37$, $F_{1,11} = 6.3$, $P = 0.03$, linear regress on all Re_f). Five of none individuals from the three-dimensional kinematics study were included in this graph (Re_f 2.1, 8.4, 12.2, 20.2, and 21.6). The remaining individuals (8 of 13) depicted were collected from the wild.

this stroke phase. At *Re* 6–12, a powerstroke during retraction occurred due to both distal flap straightening and higher speed (Fig. 6B). At $Re > 20$, the distal flap was the only source of the slight asymmetry in the VSR, where the distal flap straightening produced only an approximate 25% increase in the VSR during the 'powerstroke' compared to 'recovery' (Fig. 6C). Although the VSR may be underestimating the drag differences over half strokes at this high *Re*, the reduced asymmetry in this index is suggestive that any rowing mechanism plays a less important role as animals grow.

Individual graphs (Fig. 7) of the mean flow field are discussed above for the extreme cases, and the net flow direction relative to the stroke plane is shown in Figure 8 for the full range of Re_f investigated. Here, flow direction is nearly constant at approximately 60° for $Re_f > 8$, but decreases sharply below this Reynolds number, giving values more aligned with the stroke plane (0°).

Morphological results

The number of tracheal branches and medial lobe extension increased during ontogeny. Gills became wider with body length ($r^2 = 0.75$, $F_{1,4} = 12$, $P = 0.03$) (Fig. 3A), corresponding to a decrease in aspect ratio from 2.1 to 1.65 ($r^2 = 0.37$, $F_{1,4} = 2.3$, $P = 0.2$). Gills increased in surface area four-fold over a two-fold increase in animal length ($SA = 0.68\ L_g^{2.3}$, $r^2 = 0.99$) (Fig. 3B).

DISCUSSION

Gradual changes in Re_F, abrupt changes in stroke kinematics

Comparative studies have revealed general patterns in the way that stroke kinematics vary along the spectrum of intermediate frequency Reynolds numbers (i.e. $1 < Re_f < 100$) (Walker, 2002), with exclusive use of rowing occurring at the low end and flapping predominating at the high end. Studies of individual species that transit this *Re* range, either through ontogeny or with changes in speed, indicate that animals often use two separate appendage groups at different *Re*. For example, the copepod *Temora longicornis* forages using an equi-phase metachronal rowing stroke with its five feeding appendages ($Re_f \sim 1$), but rows with its swimming legs during escape with a metachronal power stroke and synchronized recovery stroke ($Re_f \sim 10$) (van Duren & Videler, 2003). The free-swimming mollusc, *Clione antarctica*, uses ciliary bands for low velocity movement and two flapping pteropodia for higher velocity locomotion, with the lower bound for flapping occurring at $Re_f \sim 10$ (Childress & Dudley, 2004). In these cases, the organism switches abruptly from one mechanism to another and effectively avoids a large span of the intermediate Reynolds numbers.

The mayfly *C. triangulifer* is unusual in exhibiting a change in both kinematics and apparent hydrodynamic mechanism at the same time as using a single set of appendages as they grow incrementally through the intermediate *Re* regime. Specifically, *C. triangulifer* shows a kinematic transition between a rowing and flapping mechanism over a narrow range of development as Re_f changes over the range 3–8. This transition consists of several distinct kinematic and morphological changes: the formation of a passive hinge that increases gill flexion (Fig. 4C); a dramatic decrease in pitch variation throughout the cycle (Fig. 4A); and a decrease in the stroke-plane deviation (Fig. 4B). However, some kinematic parameters do not change [cycle frequency (Table 1), inter-gill phase (Table 1), speed of protraction (Fig. 4D), and pitch during retraction] or change gradually [stroke angle maximum and minimum positions (Fig. 4E) and speed of retraction (Fig. 4D)]. Thus, even though *Centroptilum* spans the intermediate *Re* regime via gradual increases in Re_f during growth, the nymphs undergo an abrupt kinematic transition from rowing-like to flapping-like strokes near $Re_f = 5$. This suggests that the kinematic dichotomy between rowing

and flapping is not simply an artefact of comparative work that focuses largely on either low-Re or high-*Re* systems. Rather, it suggests that there is a significant hydrodynamic feature within the intermediate regime that selects against the use of intermediate kinematics.

Comparison of *Centroptilum* with other organisms

Several features of the gill system of *C. triangulifer* are unusual but the basic stroke kinematics can be compared with other animal systems at both extremes of the range *of C. triangulifer*. At the lower range of the Reynolds number scale ($Re_f < 5$), there are numerous examples of other multi-appendage array animals that use rowing stroke kinematics for propulsion, such as copepods (van Duren & Videler, 2003), remipedes (Kohlhage & Yager, 1994), ctenophores (Barlow, Sleigh & White, 1993), and *Artemia* (Williams, 1994a, b). A common feature among these examples is a change in appendage shape or profile during the recovery stroke to minimize drag and enhance net thrust. This is accomplished through articulation of the appendage (remipede), actuated flexion (cilia in the centophore) or retraction of setae on the limb (*Artemia*, remipede). In the mayfly at this Reynolds number, the gill plate is fairly stiff, with very little to no change in plate shape throughout the stroke cycle. Instead, the asymmetry in the drag on the appendage is accomplished through a change in pitch to 'feather' it during protraction (as indicated by the two times change in VSR between the power and recovery stroke, Fig. 6), as well as any mutual interaction benefit derived by the phasing of the stroke with neighboring appendages. At the high end of the viscous/inertial transition range, no multi-appendage array animals have been reported to operate with flapping mechanics. For single appendage pairs, however, there is a great deal of work on inertial-based flapping mechanisms for insect flight (Sane & Dickinson, 2002; Weis-Fogh, 1973), and, to a lesser extent, some studies investigating how such mechanisms behave or stop at a low Re_f limit (Miller & Peskin, 2004).

Significantly, most models of lift-based flapping assume inviscid flow and a concentrated source of circulation to explain the production of lift. Accordingly, one would expect lift-based mechanisms to be inoperable below a sufficiently small Re_f because of rapid frictional degradation of vorticity. Indeed, the mollusc *C. antarctica* does not use the flapping mode of locomotion below a critical value of $Re_f \sim 10$ (Childress & Dudley, 2004). Childress & Dudley (2004) constructed an idealized mathematical model of this type of locomotion, dubbed the 'Venetian blind' model, which assumed a symmetrical, time-reversible stroke motion, and found that a critical bifurcation occurred at around the same critical Reynolds number observed in *C. antarctica*. Below this value, symmetric motion could not sustain a lift-based flapping mode of propulsion. Simple mechanical experiments by Vandenberghe *et al.* (2004), supported these findings, although the bifurcation occurred at a slightly higher Re_f, possibly as a result of friction in the experimental apparatus.

There is a striking similarity between the critical Re_f observed in the preceding studies and those associated with the kinematic changes of *C. triangulifer*. However, several features of the kinematics and morphology in the mayfly violate assumptions of the Venetian blind model and the two systems may not be comparable. Specifically, the mayfly is not a time-symmetric system because of the phase lag between adjacent gills in the array, and morphology is not constant because of the development of the passive hinge that coincides with the transition in kinematics. Other hydrodynamic flapping mechanisms have been described in the literature, such as the leading edge vortex, rotational lift, added mass, and clap-and-fling models, all of which were constructed to account for the differences between the quasi-steady lift and drag forces typically found in the case of fixed-wing aerodynamics and the reality observed in the unsteady, oscillating flows generated by flapping wings (Sane & Dickinson, 2002). These mechanisms attempt to account for how vorticity (or circulation) is produced and redistributed through the flow region as a result of a fairly specific set of stroke kinematics, and so are expected to be sensitive to strong diffusion effects at a low Reynolds number. Most of these mechanisms have been noted and studied in animals that operate at much higher Re_f (typically $> 10^2$) than *C. triangulifer*, with the exception perhaps of the 'clap and fling' model first proposed by Weis-Fogh (1973) in his study of the small chalcid wasp *Encarsia formosa*. As proposed by Weis-Fogh, (1973), developed by Lighthill (1973), and subsequently confirmed by Maxworthy (1979), this mechanism uses the close proximity of two wing elements at maximum stroke to generate a strong rotational flow as the wings are drawn apart, providing a boost in lift in the early part of the stroke. This mechanism in hovering *E. formosa* occurs at $Re_f \sim 10$, which is similar to the upper range noted for *C. triangulifer*. The gill plates do approach each other closely, and are almost touching at times, so similar mechanisms may be relevant for this animal.

Gill mechanics in *Centroptilum*

Manipulation of gills in large narcotized animals (original observations) and stability in protraction speed across ontogeny (Fig. 4D) suggest that protrac-

tion may be powered by a passive elastic mechanism. Previous descriptions of the gill musculature in select mayfly species (Eastham, 1958; Brodskii, 1974; Kluge, 1989), have cited one or two muscles at this gill articulation, but dynamic characterization of gill actuation through tools such as electromyography are hampered by the small size of the taxa. The complete retraction of the gills during swimming, which flatten against the abdomen to reduce drag, may be a general feature of mayfly nymphs, including those species not utilizing active ventilation. As such, the protractive motion restoring the plates to upright position after swimming may be sufficiently actuated by a weak elastic mechanism. The active ventilation performed by the species in the present study could represent a derived function of the plates, in which the elastic mechanism is enhanced so that protraction is less limiting to the length of the stroke period (small instars), or potentially even provide useful ventilatory thrust (large instars).

Fluid-induced (passive) bending of appendages is a common feature in many wings (Wootton, 1981, 1999; Ennos, 1988), legs (Kohlhage & Yager, 1994), and gills (Eastham, 1936, 1937) and is critical to the mechanics of many rowing systems, where it functions to reduce the drag force during a recovery stroke and increase drag during the powerstroke. In insect wings, passive flexion can occur in both the chord and spanwise directions (Ennos, 1988), and wings are stiffer toward the base (Combes & Daniel, 2003). The functional significance of flexibility in flapping systems is not as obvious as in rowing, but may increase efficiency in flexible flapping by changing camber and/or pitch. Insect wings can also combine a continuous, distributed bending over an entire wing with localized flex regions created by reduced stiffness at specific points in the wing venation. The gill plates of the mayfly nymph *Leptophlebia* flex chordwise (change camber) around the gill center shaft over a half-stroke, potentially to increase drag during that phase (Eastham, 1936). However, this flexion is only on the order of 20° and occurs around the center shaft.

By contrast to *Leptophlebia*, the gills of the larger instars of *C. triangulifer* represent the first reported example of a clearly defined gill plate hinge that separates the plate into proximal and distal sections (the hinge line runs diagonally from the dorsal/root edge to the ventral/tip edge; Fig. 3A). The hinge kinematics are typically asymmetric, with a strong bias (increased bending) in the posterior direction (Fig. 4C, J). The distal flap could function as the valve of a pump consisting of three surfaces (posterior, anterior and flap) and three open sides (medial, lateral, and ventral). During the suction phase, fluid is drawn upward from the substrate. In the subsequent compression phase of the stroke, the water is squeezed out both in the ventral and dorsal directions but, because of asymmetry in the suction phase, the net result is dorsal directed transport of water. A trend from peristaltic- to valve-based pumps does occur in embryonic development of the vertebrate circulatory and lymphatic systems (Forouhar *et al.*, 2006). It has also been suggested that such biological tubular pumping systems may switch from peristaltic to a valved mechanism at some critical *Re* range because of energetic efficiency advantages (Vogel, 1992).

ACKNOWLEDGEMENTS

We thank David Funk at the Stroud Water Research Center for supplying animals. A.T.S. was supported by the Gahan Scholarship Fund (Department. of Entomology, University of Maryland) and J.W.S. acknowledges the support of the Maryland Agriculture Experiment Station. The authors are also grateful to James Duncan (Department. of Mechanical Engineering, University of Maryland) for the use of the high-speed camera equipment and Charles Mitter (Department. of Entomology, University of Maryland) for the use of microscopes. This work was supported by a grant from the National Science Foundation (CBET 0730907).

REFERENCES

Alexander RM. 1989. Optimization and gaits in the locomotion of vertebrates. *Physiological Reviews* **69:** 1199–1227.

Barlow D, Sleigh MA, White RJ. 1993. Water flows around the comb plates of the Ctenophore *Pleurobrachia* plotted by computer: a model system for studying propulsion by antiplectic metachronism. *Journal of Experimental Biology* **177:** 113–128.

Borrell BJ, Goldbogen JA, Dudley R. 2005. Aquatic wing flapping at low Reynolds numbers: swimming kinematics of the Antarctic pteropod, *Clione antarctica*. *Journal of Experimental Biology* **208:** 2939–2949.

Brennen C, Winet H. 1977. Fluid mechanics of propulsion by cilia and flagella. *Annual Review of Fluid Mechanics* **9:** 339–398.

Brodskii A. 1974. Evolution of the wing apparatus in the Ephemeroptera. *Entomological Review* **53:** 35–43.

Cannas M, Schaefer J, Domenici P, Steffensen JF. 2006. Gait transition and oxygen consumption in swimming striped surfperch *Embiotoca lateralis* Agassiz. *Journal of Fish Biology* **69:** 1612–1625.

Childress S, Dudley R. 2004. Transition from ciliary to flapping mode in a swimming mollusc: flapping flight as a bifurcation in Reω. *Journal of Fluid Mechanics* **498:** 257–288.

Combes SA, Daniel TL. 2003. Into thin air: contributions of aerodynamic and inertial-elastic forces to wing bending in the hawkmoth *Manduca sexta*. *Journal of Experimental Biology* **206:** 2999–3006.

Daniel TL, Jordan C, Grunbaum D. 1992. *Hydromechanics of swimming*. In: Alexander RM, ed. *Mechanics of Animal Locomotion*. Berlin: Springer-Verlag, 17–49.

Daniel TL, Webb PW. 1987. Physical determinants of locomotion. In: Dejours P, Bolis L, Taylor C, Weibel ER, eds. *Comparative physiology: life in water and on land*. New York, NY: Liviana Press, 343–369.

Drucker EG. 1996. The use of gait transition speed in comparative studies of fish locomotion. *American Zoologist* **36:** 555–566.

Dudley R. 2000. *The Biomechanics of Insect Flight: Form, Function, Evolution*. Princeton: Princeton University Press.

Eastham LES. 1936. The rhythmical movements of the gills of nymphal *Leptophlebia marginata* (*Ephemeroptera*) and the currents produced by them in water. *Journal of Experimental Biology* **13:** 443–449.

Eastham LES. 1937. The gill movements of nymphal *Ecdyonorus venosus* (*Ephemeroptera*) and the currents produced by them in water. *Journal of Experimental Biology* **14:** 219–228.

Eastham LES. 1958. The abdominal musculature of nymphal *Chloeon dipterum* L. (Insecta: Ephemeroptera) in relation to gill movement and swimming. *Proceedings of the Zoological Society of London* **131:** 279–291.

Ennos AR. 1988. The importance of torsion in the design of insect wings. *Journal of Experimental Biology* **140:** 137–160.

Forouhar AS, Liebling M, Hickerson A, Nasiraei-Moghaddam A, Tsai H-J, Hove JR, Fraser SE, Dickinson ME, Gharib M. 2006. The embryonic vertebrate heart tube is a dynamic suction pump. *Science* **312:** 751–753.

Fuiman L, Batty R. 1997. What a drag it is getting cold: partitioning the physical and physiological effects of temperature on fish swimming. *Journal of Experimental Biology* **200:** 1745–1755.

Funk DH, Jackson JK, Sweeney BW. 2006. Taxonomy and genetics of the parthenogenetic mayfly *Centroptilum triangulifer* and its sexual sister *Centroptilum alamance* (Ephemeroptera: Baetidae). *Journal of the North American Benthological Society* **25:** 417–429.

Gray J, Hancock GJ. 1955. The propulsion of sea-urchin spermatozoa. *Journal of Experimental Biology* **32:** 802–814.

Heglund NC, Taylor CR. 1988. Speed, stride frequency and energy cost per stride: how do they change with body size and gait? *Journal of Experimental Biology* **138:** 301–318.

Heglund NC, Taylor CR, McMahon TA. 1974. Scaling stride frequency and gait to animal size: mice to horses. *Science* **186:** 1112–1113.

Hoyt DF, Taylor CR. 1981. Gait and the energetics of locomotion in horses. *Nature* **292:** 239–240.

Kluge NJ. 1989. The problem of the homology of the tracheal gills and paranotal processi of the mayfly larvae and wings of the insects with reference to the taxonomy and phylogeny of the order Ephemeroptera *Chteniya pamyati N.A. Kholodkovskogo*. [Lectures in Memorian of N. A. Kholodkovsky], 48–77.

Kohlhage K, Yager J. 1994. An analysis of swimming in remipede crustaceans. *Philosophical Transactions: Biological Sciences* **346:** 213–221.

Lighthill J. 1976. Flagellar hydrodynamics. *SIAM Review* **18:** 161–230.

Lighthill MJ. 1973. On the Weis-Fogh mechanism of lift generation. *Journal of Fluid Mechanics* **60:** 1–17.

Maxworthy T. 1979. Experiments on the Weis-Fogh mechanism of lift generation by insects in hovering flight. Part 1. Dynamics of the 'fling'. *Journal of Fluid Mechanics Digital Archive* **93:** 47–63.

Miller LA, Peskin CS. 2004. When vortices stick: an aerodynamic transition in tiny insect flight. *Journal of Experimental Biology* **207:** 3073–3088.

Motani R. 2002. Scaling effects in caudal fin propulsion and the speed of ichthyosaurs. *Nature* **415:** 309–312.

Sane SP, Dickinson MH. 2002. The aerodynamic effects of wing rotation and a revised quasi-steady model of flapping flight. *Journal of Exprimental Biology* **205:** 1087–1096.

Spedding GR, Rosen M, Hedenstrom A. 2003. A family of vortex wakes generated by a thrush nightingale in free flight in a wind tunnel over its entire natural range of flight speeds. *Journal of Experimental Biology* **206:** 2313–2344.

Strathmann RR. 1993. Hypotheses on the origins of marine larvae. *Annual Review of Ecology and Systematics* **24:** 89–117.

Sweeney B, Funk D, Standley L. 1992. Use of the stream mayfly *Cloeon triangulifer* as a bioassay organism: life history response and body burden following exposure to technical chlordane. *Environmental Toxicology and Chemistry* **12:** 115–125.

Taylor G. 1951. Analysis of the swimming of microscopic organisms. *Proceedings of the Royal Society of London Series A, Mathematical and Physical Sciences (1934–1990)* **209:** 447–461.

Vandenberghe N, Zhang J, Childress S. 2004. Symmetry breaking leads to forward flapping flight. *Journal of Fluid Mechanics* **506:** 147–155.

van Duren LA, Videler JJ. 2003. Escape from viscosity: the kinematics and hydrodynamics of copepod foraging and escape swimming. *Journal of Experimental Biology* **206:** 269–279.

Videler JJ, Weihs D. 1982. Energetic advantages of burst-and-coast swimming of fish at high speeds. *Journal of Experimental Biology* **97:** 169–178.

Vogel S. 1992. *Vital circuits: on pumps, pipes, and the workings of circulatory systems*. Oxford: Oxford University.

Walker JA. 2002. Functional morphology and virtual models: physical constraints on the design of oscillating wings, fins, legs, and feet at intermediate Reynolds numbers. *Integrative and Comparative Biology* **42:** 232–242.

Walker JA, Westneat MW. 2002. Kinematics, dynamics, and energetics of rowing and flapping propulsion in fishes. *Integrative and Comparative Biology* **42:** 1032–1043.

Webb PW, Weihs D. 1986. Functional locomotor morphology of early life history stages of fishes. *Transactions of the American Fisheries Society* **115:** 115–127.

Weihs D. 1974. Energetic advantages of burst swimming of fish. *Journal of Theoretical Biology* **48:** 215–229.

Weis-Fogh T. 1973. Quick estimates of flight fitness in hovering animals, including novel mechanisms for lift production. *Journal of Experimental Biology* **59:** 169–230.

Williams TA. 1994a. Locomotion in developing *Artemia* larvae: mechanical analysis of antennal propulsors based on large-scale physical models: MBL. *Biological Bulletin* **187:** 156–163.

Williams TA. 1994b. A model of rowing propulsion and the ontogeny of locomotion in *Artemia* larvae: MBL. *Biological Bulletin* **187:** 164–173.

Wootton RJ. 1981. Support and deformability in insect wings. *Journal of Zoology, London* **193:** 447–468.

Wootton RJ. 1999. Invertebrate paraxial locomotory appendages: design, deformation and control. *Journal of Experimental Biology* **202:** 3333–3345.